Front. Phys. 11(5), 113101 (2016)
DOI 10.1007/s11467-016-0559-4

RESEARCH ARTICLE

Hydrogen storage in Li-doped fullerene-intercalated hexagonal boron nitrogen layers

Yi-Han Cheng[1], Chuan-Yu Zhang[1,†], Juan Ren[2], Kai-Yu Tong[1]

[1] *Physics Department, Chengdu University of Technology, Chengdu 610059, China*
[2] *School of Science, Xi'an Technological University, Xi'an 710032, China*
Corresponding author. E-mail: †*zhangchuanyu10@cdut.cn*

Received November 9, 2015; accepted December 28, 2015

New materials for hydrogen storage of Li-doped fullerene (C_{20}, C_{28}, C_{36}, C_{50}, C_{60}, C_{70})-intercalated hexagonal boron nitrogen (*h*-BN) frameworks were designed by using density functional theory (DFT) calculations. First-principles molecular dynamics (MD) simulations showed that the structures of the C_n-BN ($n = 20$, 28, 36, 50, 60, and 70) frameworks were stable at room temperature. The interlayer distance of the *h*-BN layers was expanded to 9.96–13.59 Å by the intercalated fullerenes. The hydrogen storage capacities of these three-dimensional (3D) frameworks were studied using grand canonical Monte Carlo (GCMC) simulations. The GCMC results revealed that at 77 K and 100 bar (10 MPa), the C_{50}-BN framework exhibited the highest gravimetric hydrogen uptake of 6.86 wt% and volumetric hydrogen uptake of 58.01 g/L. Thus, the hydrogen uptake of the Li-doped C_n-intercalated *h*-BN frameworks was nearly double that of the non-doped framework at room temperature. Furthermore, the isosteric heats of adsorption were in the range of 10–21 kJ/mol, values that are suitable for adsorbing/desorbing the hydrogen molecules at room temperature. At 193 K (–80 °C) and 100 bar for the Li-doped C_{50}-BN framework, the gravimetric and volumetric uptakes of H_2 reached 3.72 wt% and 30.08 g/L, respectively.

Keywords hydrogen storage, boron nitrogen, doping, first-principles, grand canonical Monte Carlo

PACS numbers 31.15.Ew, 61.72.Bb

1 Introduction

Hydrogen is considered one of the best energy carriers because of its abundance in nature and because combustion of hydrogen creates neither air pollutants nor greenhouse gases [1–3]. However, it has not been available for commercial use yet because of several hurdles that need to be overcome [4, 5]. The biggest challenge in terms of implementing a new hydrogen economy is finding materials with high gravimetric and volumetric density that can store hydrogen under favorable thermodynamic conditions and exhibit fast kinetics [1]. Among various possible storage techniques, physisorption using a porous material with a large surface area and pore volume has drawn much attention. In the past few years, many studies have been devoted to the development of materials that not only possess a porous structure and high surface area but also can reversibly store and release hydrogen under the conditions studied [6–10].

Since the early report of Novoselov *et al.* in 2004 [11], graphene, a flat monolayer of carbon atoms arranged in a two-dimensional (2D) honeycomb lattice, has rapidly become one of the hottest topics in materials science due to its fascinating properties and great potential for use in various applications. It has attracted particular attention as a gas storage material due to its specific surface area (theoretically, 2630 m^2/g) [12]. However, because of the very weak physical adsorption of H_2 for carbon-based materials, recent efforts have been directed toward non-carbon nanosystems composed of light elements such as B and N, which offer many advantages to storing hydrogen, such as the possibility of good reversibility, fast kinetics, and large surface area [13–15]. Hexagonal boron nitride (*h*-BN) is isostructural to graphite and has been referred to as "white graphene". sp^2-bonded *h*-BN shows strong covalent bonds within the plane and weak bonds with van der Waals forces between different planes. Among the pioneering works in this field, Corso *et al.* [16] successfully produced an *h*-BN nanomesh on

a Rh (1 1 1) single-crystalline surface by self-assembly. Novoselov *et al.* [17] subsequently obtained BN sheets using mechanical cleavage. These breakthrough experiments have paved the way for future application of *h*-BN sheets in gas storage, electronic devices, and templates for assembling specific nanostructures.

BN white graphene possesses a very high surface area due to its atomic-scale thin layers. Research has shown that the Brunauer–Emmett–Teller (BET) surface area is as much as 927 m^2/g with 1–4 layers of BN [18]. With the high surface area, BN white graphene exhibits high CO_2 adsorption but negligible H_2 adsorption [18]. Because of the interlayer distance in graphite (3.33–3.35 Å) [19–21] and *h*-BN (3.30–3.33 Å) [22–27], no H_2 can penetrate between the layers [28–30]. Therefore, the interlayer distance needs to be increased by other means. Here, we propose intercalating fullerenes into a two-dimensional (2D) *h*-BN structure to achieve larger interlayer distances so that the H_2 molecules can penetrate into the interlayer spaces. In the past, C_{60}-intercalated graphite was synthesized experimentally and the interlayer distance of graphite was increased from 3.37 Å to 12.7 Å [31, 32]. Kuc *et al.* theoretically proved that C_{60}-intercalated graphite can achieve a reasonable hydrogen storage capacity [33]. First-principles calculations have shown that one needs graphite with a slit pore size slightly above 6 Å for storage of H_2 in the interlayer spaces, which is in agreement with recent experimental results [28, 29, 34]. Han*et al.* reported the fabrication of lithium-organic pillared graphite with high H_2 uptakes of 4.0 wt% and 41.9 kg/m^3 at 300 K and 100 bar [35]. Very recently, Guo *et al.* designed a new Li-doped fullerene-intercalated phthalocyanine covalent organic framework designed for hydrogen storage, and the gravimetric and volumetric uptakes of H_2 reached 4.2 wt% and 18.2 g/L, respectively, at 298 K and 100 bar [36, 37].

In this study, we investigated the adsorption behavior of hydrogen in Li-doped C_n-intercalated *h*-BN frameworks using density functional theory (DFT) calculations. Our results show that the interlayer distance of the *h*-BN layers expanded to approximately 13.59 Å by the intercalated fullerenes and that the hydrogen uptakes of the Li-doped C_n-intercalated *h*-BN frameworks were nearly double that of the non-doped framework at room temperature.

2 Computational details

Using density functional theory (DFT) within the generalized gradient approximation (GGA) in the Perdew–Wang 91 (PW91) [38] and the projector-augmented wave potentials (PAW) [39] as implemented in the VASP code [40, 41], C_n-intercalated *h*-BN frameworks were optimized. The wave functions were expanded by plane waves up to a cutoff energy of 500 eV. The convergences for the energy and the force were set to 10^{-5} eV and 0.03 eV/Å, respectively. The periodic boundary condition was taken in all calculations, and the Γ point was used to represent the Brillouin zone. First-principles molecular dynamics (MD) simulations were carried out at 298 K for C_n-intercalated *h*-BN systems with the canonical NVT ensemble. The temperature was controlled using a Nosè thermostat [42], where Γ point sampling was carried out with a time step of 1 fs for 5 ps.

Hydrogen adsorption in the C_n-intercalated *h*-BN layers was simulated using GCMC simulations[43] implemented in the multipurpose simulation code Music [44]. Gas-phase fugacities for hydrogen were calculated with the Peng–Robinso equation of state. For H_2 adsorption in various sorbents, the interactions of gas–adsorbent and gas–gas were represented by the Lennard–Johns (LJ) 12-6 terms.

$$\varphi(r_{ij}) = 4\varepsilon_{ij}\left[(\sigma_{ij}/r_{ij})^{12} - (\sigma_{ij}/r_{ij})^{6}\right], \quad (1)$$

where ε_{ij} is the potential well depth and $\sigma_{ij}$is the interatomic distance at which a zero potential energy occurs, respectively, r_{ij} denotes the interaction distance between particle i and particle j. The parameters of the framework atoms were obtained from the standard DREIDING force field [45], whereas molecular hydrogen was modeled by two LJ spheres ($\sigma_H = 2.72$ Å, $\varepsilon_H/\kappa_B = 10.00$ K, $d_{H-H} = 0.74$ Å) [46]. The method in detail and the parameters of the hydrogen–lithium interaction were determined by fitting to accurate first-principles calculations as described by Guo *et al.* [36]. A number of simulation studies have revealed that the DREIDING force field can accurately predict the adsorption of light gases and diffusion and separation in porous materials [47-49]. The GCMC method was used to simulate the adsorption of H_2 molecules into the C_n-intercalated *h*-BN layers. A $3 \times 3 \times 3$ supercell was used for small C_n-intercalated *h*-BN frameworks (n = 20, 28, 36) and a $2 \times 2 \times 2$ supercell was used for large C_n-intercalated *h*-BN frameworks (n = 50, 60, 70). Van der Waals (VDW) interactions were evaluated with a cutoff radius of 12.5 Å and a computational precision of 0.001 kcal/mol. For each state, a total of 2×10^7 runs were accumulated, in which the first 1×10^7 runs were used to reach equilibrium and the remaining runs were used for calculating the ensemble averages.

The pore volumes of these C_n-intercalated *h*-BN frameworks were estimated using the method proposed by Talu and Myers [50] by using the following equation [36]:

$$V_P = N_a K_B T_0 / P. \quad (2)$$

The accessible surface areas in the designed new materials were calculated by using a numerical Monte Carlo integration technique proposed by Frost *et al.* [51] It was performed by "rolling" a probe molecule with a diameter equal to the LJ σ parameter for N_2 (3.681 Å) over the framework surface. The isosteric heat of adsorption, gravimetric density of hydrogen, and the volumetric density of hydrogen were calculated according to Refs. [52–55].

3 Results and discussion

In this work, we selected several different C_n fullerenes—C_{20} (I_h), C_{28} (T_d), C_{36} (D_{6h}), C_{50} (D_{5h}), C_{60} (I_h), and C_{70} (D_{5h})—to enlarge the distance between *h*-BN layers. We placed them in a rectangular lattice with a = 12.78 Å, b = 14.76 Å (C_{20}, C_{28}, and C_{36}), and a = 21.31 Å, b = 19.68 Å (C_{50}, C_{60}, and C_{70}). The interlayer distance of the C_n-BN frameworks was expanded to 9.96–13.59 Å by the intercalated fullerenes, which is large enough for H_2 molecules to penetrate into the interlayers. The detailed structural information of these new structures is listed in Table 1. With the increasing diameter of the fullerenes, the interlayer distance of the C_n-BN frameworks increased correspondingly. C_{50}-BN possessed the largest accessible surface of 2089.32 m^2/g, whereas C_{36}-BN showed the smallest accessible surface of 1496.84 m^2/g. Further, the stabilities of the fullerene-intercalated BN layers were evaluated at 298 K by MD simulations for 5 ps. Figures 1(a) and (b) show snapshots of the C_{28}- and C_{60}-BN frameworks during MD runs at 298 K after 5 ps. The resulting geometries show that the MD calculations predicted some fluctuations of these frameworks, especially the BN plane, due to the thermal motion of atoms at finite temperatures, but these fluctuations were not significant. Based on these results, we can conclude that these frameworks are stable at elevated temperature (298 K).

Table 1 Unit cell parameters (a, b, and c), density, pore volume (V_p), and the nitrogen accessible surface (S) of the C_n-BN frameworks.

Materials	a (Å)	b (Å)	c (Å)	Density (g/cm^3)	V_p (cm^3/g)	S (m^2/g)
C_{20}-BN	13.05	15.06	9.96	0.96	0.74	1762.77
C_{28}-BN	13.05	15.06	10.47	0.99	0.79	1656.89
C_{36}-BN	13.03	15.04	10.71	1.04	0.83	1496.84
C_{50}-BN	21.74	20.08	12.51	0.78	1.19	2089.32
C_{60}-BN	21.73	20.08	13.19	0.78	1.38	2054.14
C_{70}-BN	21.72	20.08	13.59	0.79	1.44	1995.06

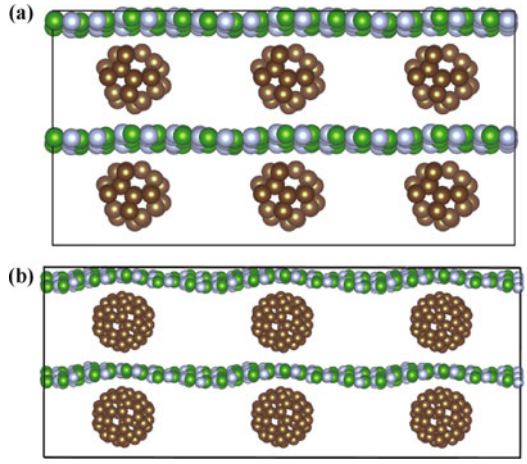

Fig. 1 Snapshots of **(a)** C_{28}-, **(b)** C_{60}-BN frameworks during MD runs at 298 K after 5 ps.

By using GCMC, we carried out a systematic simulation of hydrogen adsorption in C_n-intercalated *h*-BN frameworks. The hydrogen adsorption isotherms calculated for a pressure range of 0.1–100 bar and temperatures of 293 K and 77 K are shown in Fig. 2. The calculated gravimetric and volumetric uptakes of all sorbents at 293 K are given in Figs. 2(a) and (c), respectively. It is apparent that both the hydrogen gravimetric and volumetric uptakes increased linearly with increasing pressure of H_2 except for C_{20}-BN. The good linearity shows that the amount of hydrogen adsorbed is proportional to the pore volume and virtually independent of binding energy or surface area at room temperature. From the simulation results of six different sorbents, our results show that the highest H_2 gravimetric storage capacity and volumetric uptake were 1.21 wt% and 9.52 g/L, respectively. Corresponding to C_{20}-BN with the smallest pore volume, it is clear that both the gravimetric and the volumetric uptakes increase faster at lower pressures but slower at higher pressures. Furthermore, the gravimetric and volumetric uptakes of C_{20}-BN are higher than those of other C_n-BN (n = 28, 36, 50, 60, 70) frameworks at lower pressures. This is due to the fact that the smaller pore size produces stronger framework affinity to adsorbates at lower pressures, whereas pore volume plays a more important role at higher pressures. Figures 2(a) and (c) also show that increasing pressure causes an increase in the adsorption at room temperature, but not enough for practical use. Similarly, metal–organic frameworks (MOFs) are viewed as attractive materials for hydrogen storage because their H_2 uptake capacity decreases dramatically near room temperature [56, 57]. Temperature, of course, also has an important effect on the hydrogen storage capacity for nanoporous materials. The hydrogen adsorption capacities of new materi-

als are also investigated at very low temperatures. The gravimetric H_2 adsorption isotherms at 77 K for all C_n-intercalated BN frameworks are shown in Fig. 2(b). Our simulation results show that the gravimetric H_2uptakes at 77 K and 100 bar were 1.93, 4.87, 4.43, 6.86, 6.83, and 6.62 wt% for C_{20}-, C_{28}-, C_{36}-, C_{50}-, C_{60}-, and C_{70}-intercalated *h*-BN layers, respectively, and that the volumetric uptakes were 18.95, 50.80, 48.70, 58.01, 57.27, and 56.18 g/L, respectively. We note that C_{20}-BN reached saturation very quickly due to the small pore volume at 77 K. Our results show that C_{50}-BN had the highest H_2 gravimetric and volumetric storage capacities, with uptakes of 6.86 wt% and 58.01 g/L, respectively, at 77 K and 100 bar because it had the highest surface area and lowest density.

In order to understand the adsorption behaviors of H_2 in the frameworks on a molecular level, we examined the snapshots of the C_{50}-intercalated *h*-BN framework with H_2 molecules adsorbed at 77 K under pressures of 5 bar and 80 bar, as shown in Fig. 3. It can be seen that at low pressure, as revealed in Fig. 3(a), the H_2 molecules were mainly located on the surface of C_{50}-BN owing to the interaction of H_2 molecules with the skeleton atoms of the frameworks. As the pressure increased, as revealed in Fig. 3(b), more and more H_2 molecules begin to accommodate pore sites some distance from the surfaces of the frameworks.

As another important factor for hydrogen storage materials, the Q_{st} values calculated in this work are shown in Fig. 4. The isosteric heat of adsorption provides a measure of the strength of the interaction between hydrogen molecules and the adsorbent surface or pore structure. As shown in Fig. 4, the isosteric heats of adsorption under all pressures studied at both 293 K and 77 K are

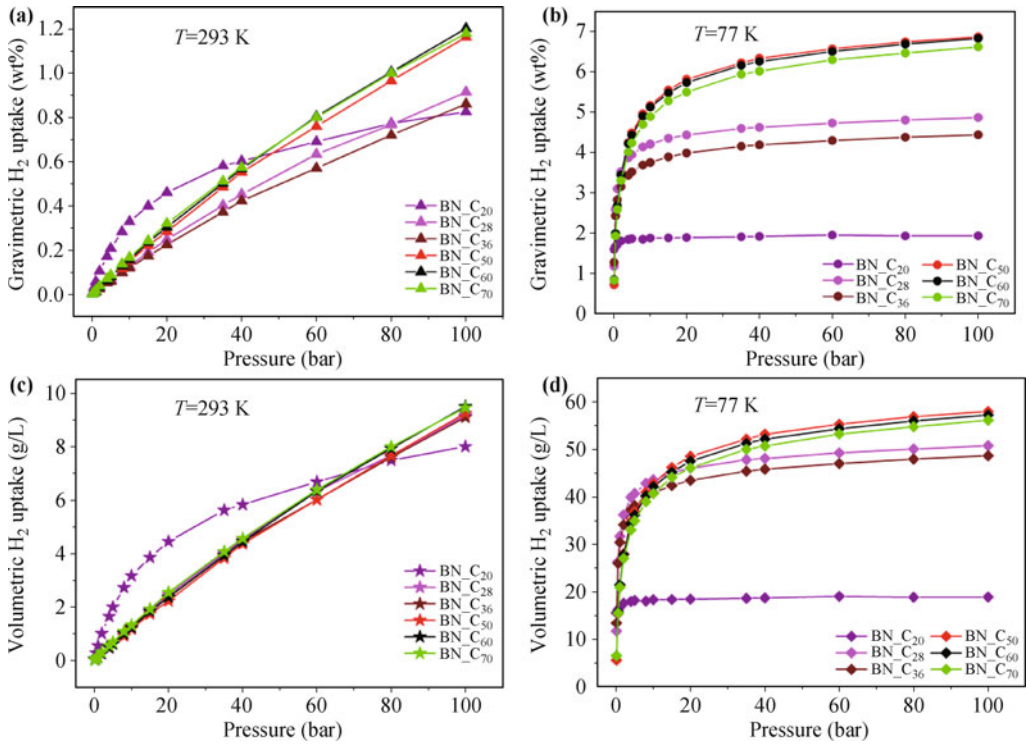

Fig. 2 Computed H_2 adsorption isotherms in C_n-intercalated *h*-BN frameworks at $T = 293$ K and $T = 77$ K in the pressure range from 0.01 to 100 bar; **(a)** H_2 gravimetric uptake at $T = 293$ K; **(b)** H_2 gravimetric uptake at $T = 77$ K; **(c)** H_2 volumetric uptake at $T = 293$K; **(d)** H_2 volumetric uptake at $T = 77$ K.

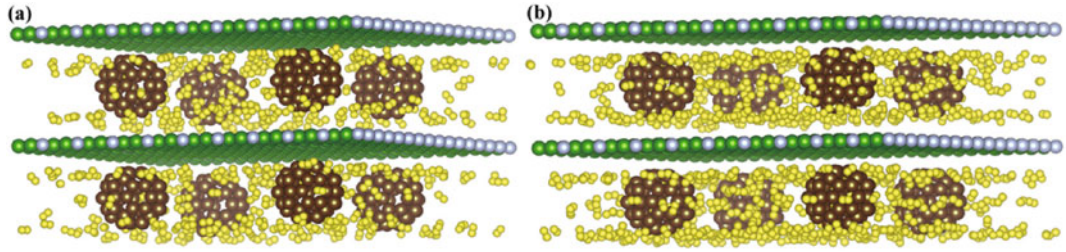

Fig. 3 The snapshots of hydrogen adsorption in C_{50}-intercalated *h*-BN framework at $T = 77$ K in the pressures of 5 bar and 80 bar. **(a)** $P = 5$ bar; **(b)** $P = 80$ bar.

in the range of 10–21 kJ/mol. From the results, we can infer that the H_2 molecules interacted with the frameworks through weak VDW interactions. It is encouraging that these values are much larger than those of any metal–organic frameworks (MOFs) or covalent organic frameworks (COFs) to data, where typical values are between 5 and 7 kJ/mol. [58] To be an ideal hydrogen storage media, we are concerned not only with charging but also with recharging. Large Q_{st} values favor efficient charging and small Q_{st} values favor recharging. In this sense, the U.S. Department of Energy (DOE) standard is meaningless because not only do we have to store a large amount of hydrogen, we also have to release it at ambient conditions. For ambient temperature, the thermodynamic requirement sets the value of Q_{st} at 15 kJ/mol. [59] The Q_{st} values of the hydrogen storage materials reported herein are in this range, which indicates that the C_n-intercalated h-BN materials achieved reliable kinetics for absorption/desorption at ambient conditions.

For comparison, we also discuss the adsorption isotherms of hydrogen in Li-doped C_n-BN systems. Previous studies [60, 61] have shown that transition metal (TM) atoms doped many materials are not stable as the strong d–d interaction between TM atoms leads to clustering. However, it has been experimentally confirmed that lithium doping provides an effective approach for enhancing H_2 uptake [62–64] owing to the strong affinity of Li^+ for the H_2 molecule. Therefore, to enhance the hydrogen storage capacities of C_n-intercalated h-BN frameworks, we further studied doping C_n-BN frameworks with Li atoms and predicted their hydrogen storage performance. We found that the Li atoms cannot be stably locate on the surface of the C_{20}-BN framework. In addition, four and eight Li atoms were bound on the hexagonal rings of the intercalated C_{28} and C_{36} fullerenes, respectively. Twelve Li atoms were bound on the pentagonal rings for all intercalated C_{50}, C_{60}, and C_{70}fullerenes. We carried out unconstrained geometry optimizations for Li-doped C_n-BN (n = 28, 36, 50, 60, 70) frameworks. The average binding energy between the Li atom and the C_n fullerenes is given by $\Delta E = \frac{1}{N}(N \times E(\mathrm{Li}) + E(\mathrm{C}_n) - E(\mathrm{Li} - \mathrm{C}_n))$, where $E(C_n)$ and $E(Li–C_n)$ are the total energies of the different fullerenes and Li adsorption on the fullerenes, respectively, E(Li) is the energy of isolated Li atoms, and N is the number of Li atoms adsorbed on each fullerene. The average binding energies of Li atoms in C_{28}, C_{36}, C_{50}, C_{60}, and C_{70} were calculated to be 3.31, 2.01, 1.84, 1.71, and 1.74 eV, respectively.

Figures 5(a) and (b) show the gravimetric and volumetric adsorption isotherms, respectively, of H_2 in Li-doped C_n-intercalated h-BN frameworks at 293 K.

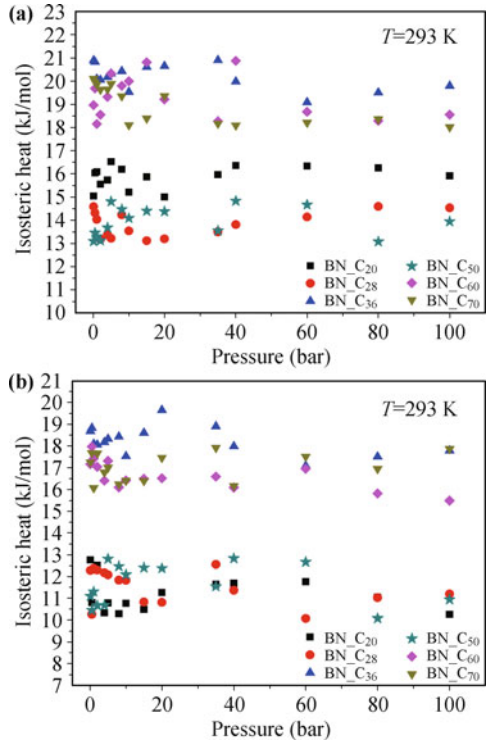

Fig. 4 Isosteric heats of hydrogen adsorption in C_n-intercalated h-BN frameworks (n = 20, 28, 36, 50, 60, and 70) at **(a)** T = 293 K and **(b)** T = 77 K.

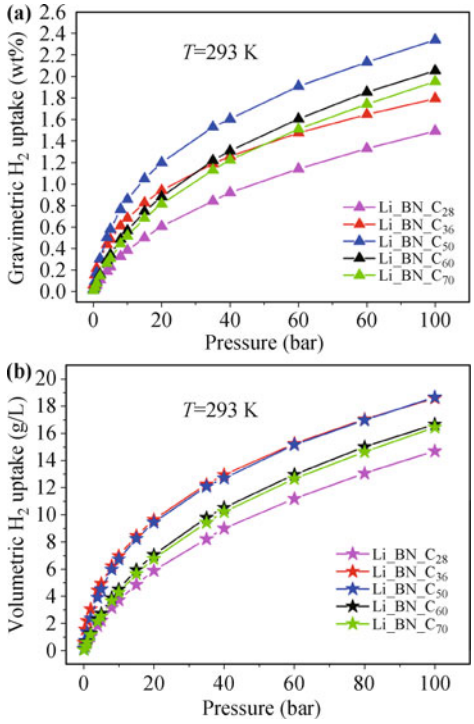

Fig. 5 Computed hydrogen adsorption isotherms in Li-doped and non-doped C_n-BN frameworks at T = 293 K in the pressure from 0.01 to 100 bar. **(a)** Gravimetric H_2 uptakes; **(b)** Volumetric H_2 uptakes.

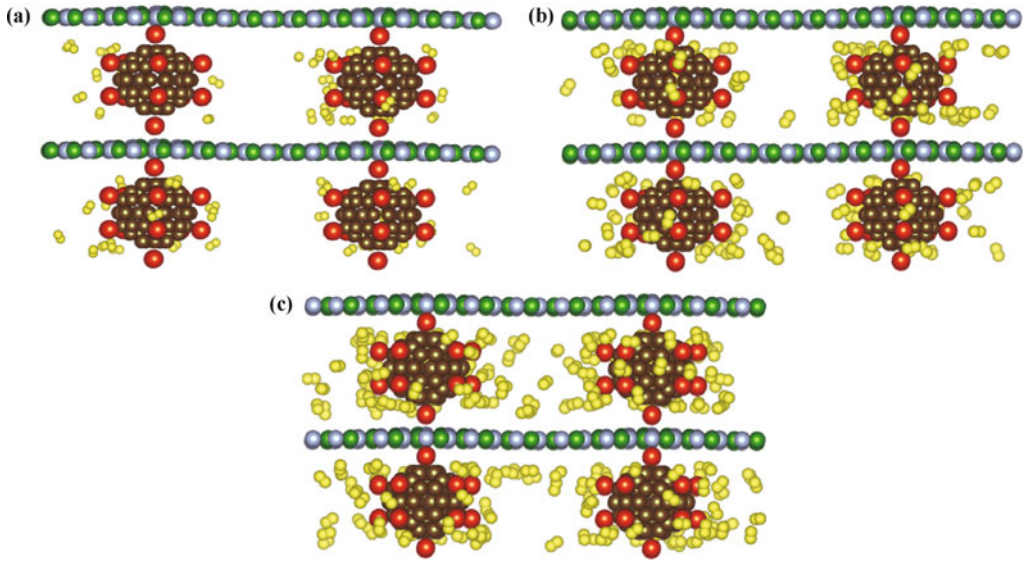

Fig. 6 The snapshots of hydrogen adsorption in Li-doped C_{50}-BN framework at $T = 293$ K in the pressure of 5, 20, and 100 bar, respectively. **(a)** $P = 5$ bar; **(b)** $P = 20$ bar; **(c)** $P = 100$ bar.

Lithium doping plays a more important role in gravimetric and volumetric adsorption. The gravimetric H_2 uptake of the Li-doped C_n-intercalated *h*-BN frameworks at 293 K and 100 bar are 1.43, 1.79, 2.34, 2.05, and 1.95 wt%, respectively, whereas the volumetric uptakes were 14.70, 18.60, 18.67, 16.67, and 16.45 g/L, respectively. Intriguingly, the gravimetric and volumetric uptakes of the Li-doped C_n-BN frameworks are approximately twice those of the non-doped framework across the whole pressure range at 293 K. Especially for the Li-doped C_{50}-BN framework, the hydrogen storage capacities reached 2.34 wt% and 18.67 g/L. The snapshots for hydrogen adsorption in the Li-doped C_{50}-BN framework at 293 K at pressures of 5, 20, and 100 bar are shown in Fig. 6. It can be seen that, at low pressure, the adsorbed H_2 molecules mainly accumulated at positions near the Li cations. As the pressure increases, the relatively large pores are also filled by H_2 molecules. In a word, Li-doped C_n-BN frameworks provide more hydrogen molecule binding sites. H_2 molecules accumulated on the surface of fullerenes coated by Li atoms leads to the enhancement in gravimetric and volumetric H_2 uptakes as compared to without doping. The underlying mechanism responsible for the high binding affinity of Li cations toward hydrogen molecules may be electrostatic charge–quadrupole and charge-induced dipole interactions.

Finally, the hydrogen storage capacities of the Li-doped C_{50}-BN framework were systematically calculated for a wide range of temperatures (77, 150, 193, 243, and 293 K) by GCMC. The results show that the gravimetric and volumetric uptakes decrease as temperature increases. At cryogenic temperatures, the hydrogen storage capacities of the Li-doped C_{50}-BN framework were 7.74 wt% and 65.40 g/L, respectively. More important is that the H_2 uptakes of the Li-doped C_{50}-BN framework can reach 3.72 wt% and 30.08 g/L at 193 K (–80 °C) and 100 bar. The hydrogen adsorptions were not saturated at 100 bar at higher temperatures (293, 243, 193, and 150 K), so with increasing pressure, the hydrogen uptakes of the Li-doped C_{50}-BN framework would be even higher.

4 Conclusions

A series of fullerene (C_{20}, C_{28}, C_{36}, C_{50}, C_{60}, C_{70})-intercalated *h*-BN frameworks were computationally designed with the aid of DFT and MD methods. As compared to our previous work [36], the interlayer distance of the *h*-BN layers was expanded to 9.96–13.59 Å by the intercalated fullerenes, which is better than experiments results (3.37–12.7 Å). The designed C_n-intercalated BN frameworks exhibited superior hydrogen storage capacity at 77 K. At 77 K and 100 bar, the highest hydrogen gravimetric and volumetric uptakes were 6.86 wt% and 58.01 g/L, respectively. The most important result is that the isosteric heats of adsorption under all pressures studied at both 293 K and 77 K were in the range of 10–21 kJ/mol. Our results also show that at 293 K and 100 bar, the highest gravimetric and volumetric uptakes of H_2 reached 2.34 wt% and 18.67 g/L, respectively, and the H_2 uptakes of the Li-doped C_{50}-BN framework reached 3.72 wt% and 30.08 g/L at 193 K (–80 °C) and 100 bar.

Acknowledgements The authors acknowledge financial support

from the National Natural Science Foundation of China (Grant No. 11404042).

References

1. L. Schlapbach and A. Züttel, Hydrogen-storage materials for mobile applications, *Nature* 414(6861), 353 (2001)
2. J. A. Turner, A realizable renewable energy future, *Science* 285(5428), 687 (1999)
3. J. A. Turner, Sustainable hydrogen production, *Science* 305(5686), 972 (2004)
4. A. W. C. van den Berg, and C. O. Arean, Materials for hydrogen storage: Current research trends and perspectives, *Chem. Commun.* 669(6), 668 (2008)
5. M. Felderhoff, C. Weidenthaler, R. von Helmolt, and U. Eberle, Hydrogen storage: The remaining scientific and technological challenges, *Phys. Chem. Chem. Phys.* 9(21), 2643 (2007)
6. H. M. El-Kaderi, J. R. Hunt, J. L. Mendoza-Cortes, A. P. Côté, R. E. Taylor, M. O'Keeffe, and O. M. Yaghi, Designed synthesis of 3D covalent organic frameworks, *Science* 316(5822), 268 (2007)
7. J. L. Belof, A. C. Stern, M. Eddaoudi, and B. Space, On the mechanism of hydrogen storage in a metal-organic framework material, *J. Am. Chem. Soc.* 129(49), 15202 (2007)
8. S. S. Han, H. Furukawa, O. M. Yaghi, and W. A. Goddard, Covalent organic frameworks as exceptional hydrogen storage materials, *J. Am. Chem. Soc.* 130(35), 11580 (2008)
9. Z. Y. Zhong, Z. T. Xiong, L. F. Sun, J. Z. Luo, P. Chen, X. Wu, J. Lin, and K. L. Tan, Nanosized nickel (or cobalt)/graphite composites for hydrogen storage, *J. Phys. Chem. B* 106(37), 9507 (2002)
10. J. Jiang, R. Babarao, and Z. Hu, Molecular simulations for energy, environmental and pharmaceutical applications of nanoporous materials: From zeolites, metal–organic frameworks to protein crystals, *Chem. Soc. Rev.* 40(7), 3599 (2011)
11. K. S. Novoselov, A. K. Geim, S. V. Morozov, D. Jiang, Y. Zhang, and S. V. Dubonos, Electric field effect in atomically thin carbon films, *Science* 306(5696), 666 (2004)
12. M. D. Stoller, S. Park, Y. Zhu, J. An, and R. S. Ruoff, Graphene-based ultracapacitors, *Nano Lett.* 8(10), 3498 (2008)
13. J. Zhou, Q. Wang, Q. Sun, P. Jena, and X. S. Chen, Electric field enhanced hydrogen storage on polarizable materials substrates, *Proc. Natl. Acad. Sci. USA* 107(7), 2801 (2010)
14. M. Khazaei, M. S. Bahramy, N. S. Venkataramanan, H. Mizuseki, and Y. Kawazoe, Chemical engineering of prehydrogenated C and BN-sheets by Li: Application in hydrogen storage, *J. Appl. Phys.* 106(9), 094303 (2009)
15. L. P. Zhang, P. Wu, and M. B. Sullivan, Hydrogen adsorption on Rh, Ni, and Pd functionalized single-walled boron nitride nanotubes, *J. Phys. Chem. C* 115(10), 4289 (2011)
16. M. Corso, W. Auwärter, M. Muntwiler, A. Tamai, T. Greber, and J. Osterwalder, Boron nitride nanomesh, *Science* 303(5655), 217 (2004)
17. K. S. Novoselov, D. Jiang, F. Schedin, T. J. Booth, V. V. Khotkevich, S. V. Morozov, and A. K. Geim, Two-dimensional atomic crystals, *Proc. Natl. Acad. Sci. USA* 102(30), 10451 (2005)
18. A. Nag, K. Raidongia, K. P. S. S. Hembram, R. Datta, U. V. Waghmare, and C. N. R. Rao, Graphene analogues of BN: Novel synthesis and properties, *ACS Nano* 4(3), 1539 (2010)
19. J. D. Bernal, The structure of graphite, *Proc. R. Soc. Lond. A* 106(740), 749 (1924)
20. D. Chung, Review graphite, *J. Mater. Sci.* 37(8), 1475 (2002)
21. Y. Baskin and L. Meyer, Lattice constants of graphite at low temperatures, *Phys. Rev.* 100(2), 544 (1955)
22. V. L. Solozhenko, G. Will, and F. Elf, Isothermal compression of hexagonal graphite-like boron nitride up to 12 GPa, *Solid State Commun.* 96(1), 1 (1995)
23. W. Paszkowicz, J. B. Pelka, M. Knapp, T. Szyszko, and S. Podsiadlo, Lattice parameters and anisotropic thermal expansion of hexagonal boron nitride in the 10–297.5 K temperature range, *Appl. Phys. A* 75(3), 431 (2002)
24. A. Marini, P. Garcia-Gonzalez, and A. Rubio, First-principles description of correlation effects in layered materials, *Phys. Rev. Lett.* 96(13), 136404 (2006)
25. G. Kern, G. Kresse, and J. Hafner, Ab initio calculation of the lattice dynamics and phase diagram of boron nitride, *Phys. Rev. B* 59(13), 8551 (1999)
26. R. Pease, An X-ray study of boron nitride, *Acta Crystallogr.* 5(3), 356 (1952)
27. Y. Shi, C. Hamsen, X. Jia, K. K. Kim, A. Reina, M. Hofmann, A. L. Hsu, K. Zhang, H. Li, Z.Y. Juang, M. S. Dresselhaus, L. J. Li, and J. Kong, Synthesis of few-layer hexagonal boron nitride thin film by chemical vapor deposition, *Nano Lett.* 10(10), 4134 (2010)
28. S. S. Han, H. S. Kim, K. S. Han, J. Y. Lee, H. M. Lee, J. K. Kang, S. I. Woo, A. C. T. van Duin, and W. A. Goddard, Nanopores of carbon nanotubes as practical hydrogen storage media, *Appl. Phys. Lett.* 87(21), 213113 (2005)
29. S. Patchkovskii, J. S. Tse, S. N. Yurchenko, L. Zhechkov, T. Heine, and G. Seifert, Graphene nanostructures as tunable storage media for molecular hydrogen, *Proc. Natl. Acad. Sci. USA* 102(30), 10439 (2005)
30. W. Q. Deng, X. Xu, and Goddard, New alkali doped pillared carbon materials designed to achieve practical reversible hydrogen storage for transportation, *Phys. Rev. Lett.* 92(16), 166103 (2004)
31. M. S. Fuhrer, J. G. Hou, X. D. Xiang, and A. Zettl, C_{60} intercalated graphite: Predictions and experiments, *Solid State Commun.* 90(6), 357 (1994)
32. V. Gupta, P. Scharff, K. Risch, H. Romanus, and R. Müller, Synthesis of C_{60} intercalated graphite, *Solid State Commun.* 131(3–4), 153 (2004)

33. A. Kuc, L. Zhechkov, S. Patchkovskii, G. Seifert, and T. Heine, Hydrogen sieving and storage in fullerene intercalated graphite, *Nano Lett.* 7(1), 1 (2007)
34. Y. Gogotsi, R. K. Dash, G. Yushin, T. Yildirim, G. Laudisio, and J. E. Fischer, Tailoring of nanoscale porosity in carbide-derived carbons for hydrogen storage, *J. Am. Chem. Soc.* 127(46), 16006 (2005)
35. S. S. Han and S. S. Jang, A hydrogen storage nanotank: Lithium-organic pillared graphite, *Chem. Commun.* 36(36), 5427 (2009)
36. J. H. Guo, H. Zhang, and Y. Miyamoto, New Li-doped fullerene-intercalated phthalocyanine covalent organic frameworks designed for hydrogen storage, *Phys. Chem. Chem. Phys.* 15(21), 8199 (2013)
37. J. Ren, H. Zhang, and X. L. Cheng, Grand canonical Monte Carlo simulation of isotherm for hydrogen adsorption on nanoporous $LiBH_4$, *Comput. Mater. Sci.* 71, 109 (2013)
38. J. P. Perdew, J. A. Chevary, S. H. Vosko, K. A. Jackson, M. R. Pederson, D. J. Singh, and C. Fiolhais, Atoms, molecules, solids, and surfaces: Applications of the generalized gradient approximation for exchange and correlation, *Phys. Rev. B* 46(11), 6671 (1992)
39. P. E. Blöchl, Projector augmented-wave method, *Phys. Rev. B* 50(24), 17953 (1994)
40. G. Kresse and J. Hafner, Norm-conserving and ultrasoft pseudopotentials for first-row and transition elements, *J. Phys. Condens. Matter* 6(40), 8245 (1994)
41. G. Kresse and D. Joubert, From ultrasoft pseudopotentials to the projector augmented-wave method, *Phys. Rev. B* 59(3), 1758 (1999)
42. S. Nosé, A molecular dynamics method for simulations in the canonical ensemble, *Mol. Phys.* 52(2), 255 (1984)
43. D. Frenkel and B. Smit, Understanding Molecular Simulation, *Computational Science Series*, San Diego: Academic Press, 2002
44. A. Gupta, S. Chempath, M. J. Sanborn, L. A. Clark, and R. Q. Snurr, Object-oriented programming paradigms for molecular modeling, *Mol. Simul.* 29(1), 29 (2003)
45. S. L. Mayo, B. D. Olafson, and Goddard, Dreiding: A generic force field for molecular simulations, *J. Phys. Chem.* 94(26), 8897 (1990)
46. Q. Y. Yang and C. L. Zhong, Molecular simulation of adsorption and diffusion of hydrogen in metal-organic frameworks, *J. Phys. Chem. B* 109(24), 11862 (2005)
47. G. Garberoglio, A. I. Skoulidas, and J. K. Johnson, Adsorption of gases in metal organic materials: Comparison of simulations and experiments, *J. Phys. Chem. B* 109(27), 13094 (2005)
48. T. Düren, L. Sarkisov, O. M. Yaghi, and R. Q. Snurr, Design of new materials for methane storage, *Langmuir* 20(7), 2683 (2004)
49. B. Assfour and G. Seifert, Adsorption of hydrogen in covalent organic frameworks: Comparison of simulations and experiments, *Microporous Mesoporous Mater.* 133(1–3), 59 (2010)
50. O. Talu and A. L. Myers, Molecular simulation of adsorption: Gibbs dividing surface and comparison with experiment, *AIChE J.* 47(5), 1160 (2001)
51. H. Frost, T. Düren, and R. Q. Snurr, Effects of surface area, free volume, and heat of adsorption on hydrogen uptake in metal-organic frameworks, *J. Phys. Chem. B* 110(19), 9565 (2006)
52. R. Q. Snurr, A. T. Bell, and D. N. Theodorou, Prediction of adsorption of aromatic hydrocarbons in silicalite from grand canonical Monte Carlo simulations with biased insertions, *J. Phys. Chem.* 97(51), 13742 (1993)
53. H. Tanaka, J. Fan, H. Kanoh, H. Yudasaka, S. Iijima, and K. Kaneko, Quantum nature of adsorbed hydrogen on single-wall carbon nanohorns, *Mol. Simul.* 31(6–7), 465 (2005)
54. D. Levesque, A. Gicquel, F. L. Darkrim, and S. B. Kayiran, Monte Carlo simulations of hydrogen storage in carbon nanotubes, *J. Phys. Condens. Matter* 14(40), 9285 (2002)
55. P. Kowalczyk, H. Tanaka, R. Hołyst, K. Kaneko, T. Ohmori, and J. Miyamoto, Storage of hydrogen at 303 K in graphite slitlike pores from grand canonical Monte Carlo simulation, *J. Phys. Chem. B* 109(36), 17174 (2005)
56. B. Panella, M. Hirscher, H. Pütter, and U. Müller, Hydrogen adsorption in metal–organic frameworks: Cu-MOFs and Zn-MOFs compared, *Adv. Funct. Mater.* 16(4), 520 (2006)
57. Y. W. Li and R. T. Yang, Hydrogen storage in metal-organic frameworks by bridged hydrogen spillover, *J. Am. Chem. Soc.* 128(25), 8136 (2006)
58. L. J. Murray, M. Dincă, and J. R. Long, Hydrogen storage in metal–organic frameworks, *Chem. Soc. Rev.* 38(5), 1294 (2009)
59. S. K. Bhatia and A. L. Myers, Optimum conditions for adsorptive storage, *Langmuir* 22(4), 1688 (2006)
60. K. Srinivasu, K. R. S. Chandrakumar, and S. K. Ghosh, Quantum chemical studies on hydrogen adsorption in carbon-based model systems: Role of charged surface and the electronic induction effect, *Phys. Chem. Chem. Phys.* 10(38), 5832 (2008)
61. Q. Sun, Q. Wang, P. Jena, and Y. Kawazoe, Clustering of Ti on a C_{60} surface and its effect on hydrogen storage, *J. Am. Chem. Soc.* 127(42), 14582 (2005)
62. K. L. Mulfort and J. T. Hupp, Chemical reduction of metal-organic framework materials as a method to enhance gas uptake and binding, *J. Am. Chem. Soc.* 129(31), 9604 (2007)
63. D. Himsl, D. Wallacher, and M. Hartmann, Improving the hydrogen-adsorption properties of a hydroxy-modified MIL-53 (Al) structural analogue by lithium doping, *Angew. Chem. Int. Ed.* 48(25), 4639 (2009)
64. Z. H. Xiang, Z. Hu, W. T. Yang, and D. P. Cao, Lithium doping on metal-organic frameworks for enhancing H_2 storage, *Int. J. Hydrogen Energy* 37(1), 946 (2012)